Quantitative Kinetics of [124I]FIAU in Cat and Man

Andreas Jacobs, Ines Bräunlich, Rudolf Graf, Martin Lercher, Takayuki Sakaki, Jürgen Voges, Volker Hesselmann, Wolfgang Brandau, Klaus Wienhard, and Wolf-Dieter Heiss

Max-Planck-Institute for Neurological Research, Center for Molecular Medicine, and Departments of Neurology, Stereotactic Neurosurgery, and Radiology, University of Cologne, Cologne; and Department of Nuclear Chemistry and Radiopharmacy, University of Essen, Essen, Germany

For the assessment of the efficacy of clinical gene therapy trials, different imaging modalities have been developed that enable a noninvasive assessment of location, magnitude, and duration of transduced gene expression in vivo. These imaging methods rely on a combination of an appropriate marker gene and a radiolabeled or paramagnetic marker substrate that can be detected by PET or MRI. Here, we assess whether the nucleoside analog 2′-fluoro-2′-deoxy-1β-D-arabinofuranosyl-5-iodouracil (FIAU), a specific marker substrate for herpes simplex virus type 1 thymidine kinase (HSV-1-*tk*) gene expression, penetrates the blood–brain barrier (BBB) as an essential prerequisite for a noninvasive assessment of HSV-1-*tk* gene expression in gliomas. **Methods:** No-carrier-added [124I]FIAU was synthesized by reacting the precursor 2′-fluoro-2′-deoxy-1β-D-arabinofuranosyluracil (FAU) with carrier-free [124I]NaI. The course of biodistribution of [124I]FIAU was investigated in anesthetized cats ($n = 3$; organs) and in one patient with a recurrent glioblastoma (plasma and brain) by PET imaging over several hours (cats, 1–22 h) to several days (patient, 1–68 h). FIAU PET was performed in conjunction with multitracer PET imaging (cerebral blood flow and cerebral metabolic rate of O_2 in cats only; cerebral metabolic rate of glucose and [11C]methionine in all subjects). A region-of-interest analysis was performed on the basis of coregistered high-resolution MR images. The average radioactivity concentration was determined, decay corrected, and recalculated as percentage injected dose per gram of tissue (%ID/g) or as standardized uptake values (SUVs). **Results:** The average chemical yield of [124I]FIAU synthesis was 54.6% ± 6.8%. The chemical and radiochemical purities of [124I]FIAU were found to be >98% and >95%, respectively. In cats, the kinetic analysis of [124I]FIAU-derived radioactivity showed an early peak (1–2 min after injection) in heart and kidneys (0.20 %ID/g; SUV, 4.0) followed by a second peak (10–20 min after injection) in liver and spleen (0.16 %ID/g; SUV, 3.2) with subsequent clearance from tissues and a late peak in the bladder (10–15 h after injection). In the unlesioned cat brain, no substantial [124I]FIAU uptake occurred throughout the measurement (<0.02 %ID/g; SUV, <0.4). In the patient, [124I]FIAU uptake in normal brain was also very low (<0.0002 %ID/g; SUV, <0.16). In contrast, the recurrent glioblastoma revealed relatively high levels of [124I]FIAU-derived radioactivity (5–10 min after injection; 0.001 %ID/g; SUV, 0.8), which cleared slowly over the 68-h imaging period. **Conclusion:** The PET marker substrate FIAU does not penetrate the intact BBB significantly and, hence, is not the marker substrate of choice for the noninvasive localization of HSV-1-*tk* gene expression in the central nervous system under conditions in which the BBB is likely to be intact. However, substantial levels of [124I]FIAU-derived radioactivity may occur within areas of BBB disruption (e.g., glioblastoma), which is an essential prerequisite for imaging clinically relevant levels of HSV-1-*tk* gene expression in brain tumors after gene therapy by FIAU PET. For this purpose, washout of nonspecific radioactivity should be allowed for several days.

Key Words: 2′-fluoro-2′-deoxy-1β-D-arabinofuranosyl-5-iodouracil; tracer kinetics; PET; molecular imaging; gene therapy

The design of effective gene therapy strategies relies on concerted research to define the genetic and pathophysiologic alterations causing the disease, to understand the biologic characteristics of the target tissue, and to develop safe vector and expression systems to achieve efficient, targeted, and regulated alteration of specific therapeutic gene expression. Many schemes for gene therapy for hereditary and acquired diseases have been envisioned, but several issues such as the best vector, vector toxicity, transgene or modified cell line stability, the best promoters, and how much and when to apply must be worked out (*1*). Clinical gene therapy trials for recurrent glioblastomas revealed that transduction of the herpes simplex virus type 1 thymidine kinase gene (HSV-1-*tk*) with subsequent prodrug activation (ganciclovir) as an adjuvant to the surgical resection could be performed safely. However, clinical responses were observed in only a few patients with very small brain tumors (*2,3*). One of the most important issues for making gene therapy widely applicable to humans is the development of technology for the noninvasive monitoring of the location, magnitude, and duration of transgene expression in vivo (*4–6*). The Recombinant DNA Advisory Committee has called for better assays for measuring transgene expression in cells and tissues, especially in view of the first person who died from liver-directed adenovirus vector-mediated

gene therapy (7). Therefore, noninvasive monitoring of the distribution of transgene expression over time is highly desirable and could have a critical impact on the safety and assessment of the efficiency of gene therapy in its clinical application.

Noninvasive localization of the magnitude and duration of gene expression relies on the transduction of marker genes encoding enzymes or receptors leading to a regional accumulation of radiolabeled or paramagnetic marker substrates (4,6,8–13) or receptor-binding compounds (10,14,15) that can be detected by radionuclide imaging or MRI. Radiolabeled 2′-fluoro-2′-deoxy-1β-D-arabinofuranosyl-5-iodouracil (FIAU), a specific substrate for HSV-1 thymidine kinase (HSV-1-TK), and PET have been used successfully for the noninvasive localization of different levels of HSV-1-*tk* gene expression after ex vivo or in vivo retroviral (11,12), adenoviral (8,13), and herpes viral (16) vector-mediated gene transduction in subcutaneous tumor models in nude rats or mice.

FIAU is a thymidine nucleoside analog that has been developed as an antiviral agent because of its activity against herpes and hepatitis viruses (17). There is selective initial phosphorylation of FIAU by virally encoded thymidine kinase. FIAU-monophosphate is further phosphorylated to di- and triphosphate by cellular kinases. FIAU-triphosphate causes selective inhibition of viral replication. In a clinical evaluation for its use as a treatment for chronic hepatitis B, long-term oral administration of FIAU resulted in severe multiorgan toxicity, characterized by a delayed onset and refractory lactic acidosis caused by interference with mitochondrial DNA polymerase γ (18,19). However, diagnostic doses of FIAU for imaging HSV-1-*tk* gene expression are lower by a factor of $<10^{-6}$ than the daily doses in the hepatitis B trials in which no FIAU-related toxicity was observed (19). Therefore, clinical application should be safe (11).

The lipophilic properties of FIAU predicted its good blood–brain barrier (BBB) penetration (20–22). However, an organ dosimetry evaluation in rats injected with diagnostic doses of [124I]FIAU revealed very low values for [124I]FIAU-derived radioactivity within the brain, suggesting limited BBB penetration (12). To further evaluate the applicability of [124I]FIAU as a potential marker substrate to image HSV-1-*tk* gene expression in the human central nervous system (CNS) with special reference to its penetration of the BBB, we describe quantitative kinetics of [124I]FIAU in three healthy cats and one patient with a recurrent glioblastoma.

MATERIALS AND METHODS

Radiochemical Synthesis

No-carrier-added 124I was produced from enriched 124Te oxide by the 124Te(d,2n)124I reaction (CV28 cyclotron; Cyclotron Corp., Berkeley, CA) and subjected to dry distillation at 740°C (23). The released 124I was trapped in 200 μL 0.02N NaOH. For radiochemical synthesis of [124I]FIAU, the precursor 2′-fluoro-2′-desoxy-1β-D-arabinofuranosyluracil (FAU; 0.3 mg) (Hartmann Analytic

GmbH, Braunschweig, Germany) was dissolved in 2 mol/L HNO_3 (100 μL) and heated at 115°C with carrier-free [124I]NaI (80–130 μL) for 45 min. After cooling and neutralization (0.1 concentrated ammonia; 100 μL), the solution was purified by preparative high-performance liquid chromatography (HPLC) (Knauer solvent pump K1001 [Berlin, Germany] combined with an ultraviolet detector [λ, 254 nm] and a Geiger-Müller detector [Berthold, Wildbad, Germany]) using an isocratic solvent system of 10% ethanol in 50 mmol/L NaH_2PO_4 at pH 5.3 (Adsorbosil RP C_{18} 5-μm column [Alltech, Unterhaching, Germany]; 250 × 4.6 mm; flow, 1 mL/min). The FIAU fraction was diluted with sterile physiologic saline solution to reduce the concentration of ethanol to 5% and passaged through a 0.22-μm filter. The radiochemical purity was determined by radio–thin-layer chromatography (Poly-gram Sil-G UV254 [Macherey-Nagel, Düren, Germany]; eluent: ethyl acetate, acetone, and water [14:8:1]) and analytic HPLC using an isocratic solvent system of 10% methanol in 50 mmol/L K_2HPO_4 at pH 4.3 (Econosil RP C_8 5-μm column [Alltech]; 250 × 4.6 mm; flow, 1 mL/min).

PET and MRI Investigations in Cats

The experimental procedures were in accordance with the German Laws for Animal Protection and were approved by the local animal care committee and the Bezirksregierung Cologne. Halo-thane-anesthetized male cats ($n = 3$), weighing 2500–3000 g, underwent a tracheotomy for ventilation. Arterial and venous lines were placed for the continuous assessment of arterial blood pressure and partial pressure of O_2 in arterial blood. A urinary catheter was inserted for sampling of excreted nonmetabolized [124I]FIAU. Twenty-four hours after intraperitoneal injection of 15 mL 0.9% NaI to block thyroid uptake of radioactive iodide, no-carrier-added [124I]FIAU (37 MBq [1 mCi] per animal) was injected intravenously, and thereafter PET was performed for 8 h ($n = 1$) or 22 h ($n = 2$). Animals were then killed and frozen at −20°C without changing their position, and T1-weighted high-resolution MR images were obtained on a Phillips ACS scanner (Hamburg, Germany) and coregistered to the summed [124I]FIAU PET as described (24). Before [124I]FIAU PET, additional multitracer PET imaging ([18F]FDG, [15O]H_2O, [15O]O_2, and [11C]methionine ([11C]MET)) was performed on two animals as described (25) (Fig. 1).

Patient Study

A 50-y-old male patient, who had been treated for a glioblastoma in the left subcortical parieto-occipital region (surgery, chemotherapy, and radiotherapy), presented 3 mo after his last operation with a new onset of right-sided hemiparesis and radiologic and histologic (stereotactic biopsy) signs of a recurrent glioblastoma. After approval of the study protocol by the local ethics committee, signed informed consent was obtained, and the patient underwent high-resolution MRI, FDG PET, and [11C]MET PET imaging on 3 subsequent days. FDG PET and [11C]MET PET were performed after an intravenous bolus injection of 370 MBq (10 mCi) FDG and 740 MBq (20 mCi) [11C]MET, respectively; details of the imaging protocols are described elsewhere (26,27). After blockade of the thyroid by oral administration of sodium perchlorate for 3 d, FIAU PET was performed after an intravenous bolus injection of 77.7 MBq (2.1 mCi) [124I]FIAU. FIAU PET, FDG PET, and [11C]MET PET as well as MR images were coregistered (24). Radioactivity was counted in multiple plasma samples at various times after [124I]FIAU administration using a cross-calibrated γ counter (MAG 312; Berthold).
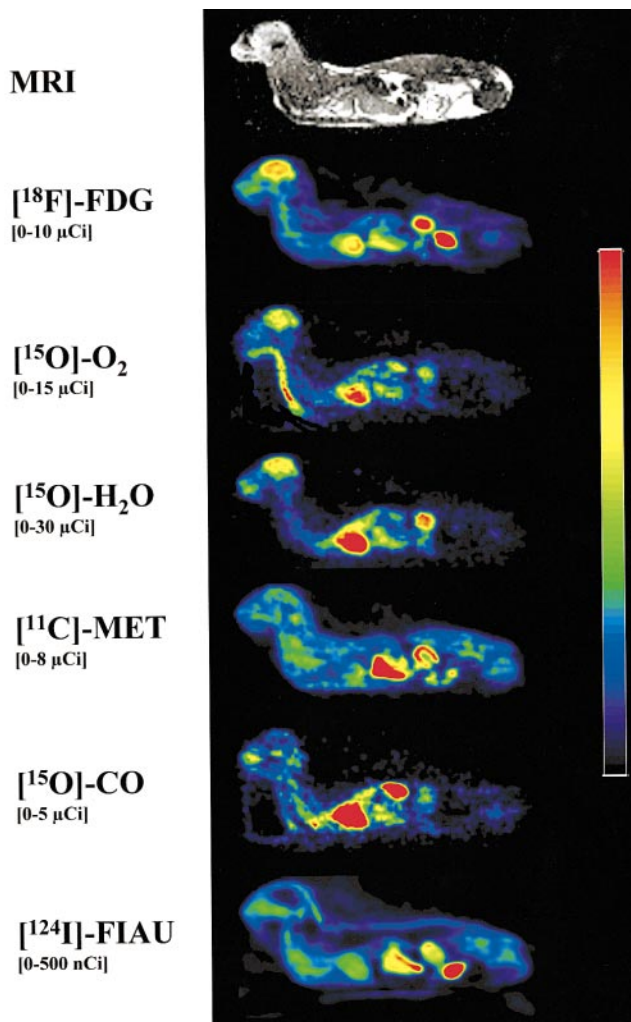
FIGURE 1. Multitracer PET imaging of ventilated cat allows functional analysis of various tissues of total body at same physiologic status over prolonged period of time using specific radiotracers. Coregistered MRI allows anatomic delineation of various organs. In healthy cat brain, physiologic glucose ([^{18}F]FDG) and oxygen ([^{15}O]O$_2$) consumption with normal cerebral blood flow ([^{15}O]H$_2$O) is not accompanied by significant uptake of amino acid ([^{11}C]MET) or nucleoside analog ([^{124}I]FIAU).

[^{124}I]FIAU PET Measurement

[^{124}I]FIAU tracer accumulation and washout were recorded from the entire animal (cats) or the entire brain and soft tissue of the head (patient) with an ECAT EXACT HR tomograph (CTI/Siemens PET Systems, Knoxville, TN; 47 transaxial slices; full width at half maximum, 3.6 mm (28)). Transmission scans were obtained with rotating ^{68}Ge rod sources in two-dimensional mode for 10 min. A dynamic series of emission scans was obtained in two-dimensional mode (cats) or three-dimensional mode (patient). Each scan was corrected for randoms, dead time, attenuation, and scatter. Emission scans (duration, 30 s to 60 min) were obtained in cats starting immediately after [^{124}I]FIAU injection for 8 h ($n = 1$) or 22 h ($n = 2$). Emission scans (duration, 30 s to 10 min) were obtained in the patient starting immediately after [^{124}I]FIAU injection for 1 h. Thereafter, transmission (10 min) and emission (50 min) scans were obtained at 8, 20, 24, 30, 44, and 68 h after

[^{124}I]FIAU injection, resulting in one set of kinetic FIAU PET frames within the first hour and six additional FIAU PET images. Images were reconstructed using an iterative reconstruction method (Fourier rebinning followed by two-dimensional ordered subsets expectation maximum [OSEM]) with measured attenuation correction, smoothed with an 8-mm Gaussian filter. The OSEM reconstruction parameters were 32 subsets, four iterations in a 128 × 128 matrix using standard ECAT 7 software (CTI/Siemens).

Evaluation of Data

Data evaluation was based on a region-of-interest (ROI) analysis of coregistered MR/PET images (24). ROIs were outlined to represent various organs in the cat (brain, heart, lung, muscle, liver, stomach, spleen, intestine, kidney, and bladder; Fig. 2). The ROI analysis in the patient focused on various regions in the brain
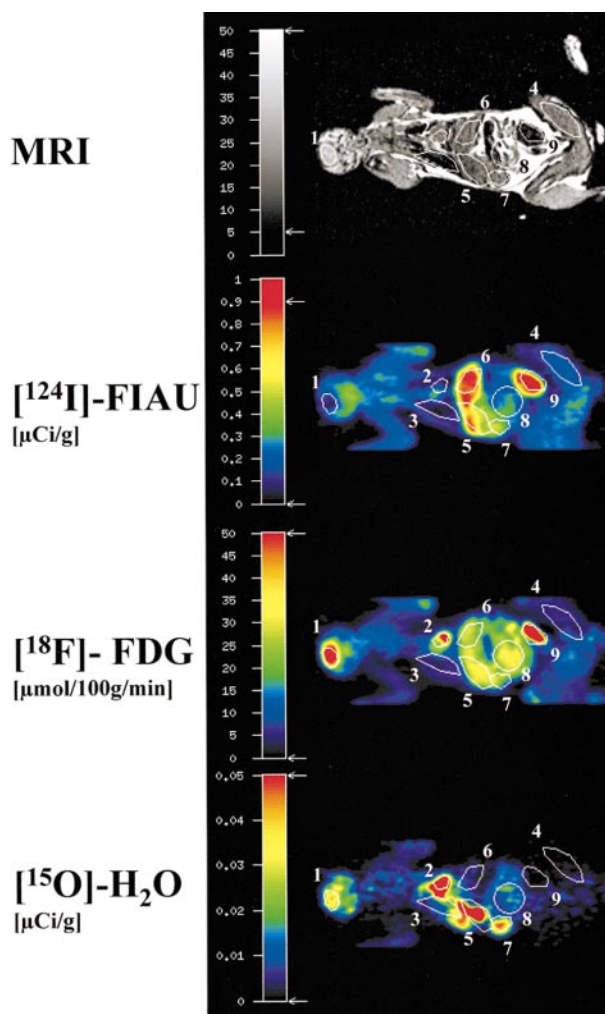

FIGURE 2. For dynamic evaluation of [^{124}I]FIAU influx and washout in cats, ROI analysis focused on organs such as brain (1), heart (2), lung (3), muscle (4), liver (5), stomach and spleen (6), kidney (7), intestine (8), and bladder (9). Stomach and intestine could not be differentiated and were combined into one region. Coregistered FDG PET reveals glucose consumption in brain and heart and excretion of tracer into bladder. Coregistered [^{15}O]H$_2$O PET shows high activities in well-perfused organs such as brain, heart, liver, and kidneys.

and nonbrain tissue (tumor, paratumor, gray matter, white matter, and scalp). For each of these regions or volumes of interest (VOIs = sum of ROIs over three adjacent slices, extending over 9.375 mm) and for each time frame, the average radioactivity concentration (nCi/g) was calculated. These data were decay corrected and divided by total injected dose (ID) to represent percentage ID per gram (%ID/g) values or divided by the ratio of total ID and body weight to represent standardized uptake values (SUVs). The %ID/g values or SUVs were plotted as time–activity curves. In cats, these time–activity curves were averaged over the three animals. In the patient, the tissue time–activity curves were generated to illustrate the different tracer uptake patterns in the tumor and normal brain tissue. The time course of radioactivity in each VOI was fitted using various kinetic models including a two-rate constant, one-tissue compartment model and a three-rate constant, two-tissue compartment model and the plasma volume contribution as an additional parameter as described (29). Nonlinear least-square fitting was done with a modified gradient-expansion algorithm (30). The best fits were determined by minimizing a χ^2 function with respect to variations in the model parameters. Patlak plots were used to standardize the kinetics of tissue radioactivity to the kinetics of plasma radioactivity as described (29,31). In brief, the ratio of

$$Y = C_{VOI}(t)/C_{Plasma}(t)$$

was plotted against a modified time:

$$\Theta(t) = \left[\int_0^t C_{Plasma}(\tau)d\tau \right] / C_{Plasma}(t),$$

where $C_{VOI}(t)$ and $C_{Plasma}(t)$ are the tissue and plasma radioactivity concentrations at time t, respectively. This method simulates the uptake temporal pattern that would result from a plasma radioactivity concentration that is constant over time. For a tracer with no irreversible accumulation, this graphic method typically results, after an initial distribution phase, in a steady state of specific tissue radioactivity (Y) with time (Θ). For a tracer with irreversible trapping, tissue radioactivity shows a linear increase (29,31).

RESULTS

Radiochemical Synthesis

The average chemical yield of [124I]FIAU synthesis was 54.8% ± 6.8%. The chemical and radiochemical purities of [124I]FIAU were found to be >98% and >95%, respectively. The theoretic specific activity of [124I]FIAU was calculated to be 31.1 Ci/μmol.

[124I]FIAU Does Not Penetrate Intact BBB in Healthy Cats

Multitracer PET imaging and MRI of the continuously ventilated cat allows simultaneous assessment of various physiologic parameters of the brain such as cerebral metabolic rate of glucose, cerebral metabolic rate of O_2, cerebral blood flow, cerebral blood volume, and methionine uptake as well as the identification of the various organs for a whole-body kinetic analysis of a new tracer such as [124I]FIAU (Fig. 1). ROI analysis was performed on coronal body slices as outlined in Figure 2. Tracer regions were

drawn over the whole brain and heart, one side of the lung, muscle, liver, one kidney, intestine, and bladder; stomach and spleen could not be differentiated exactly and were combined into one ROI. The kinetic analysis of [124I]FIAU in vivo (calculated as mean %ID/g from three [first 8 h] and two [9–22 h] animals) showed an early peak (1–2 min after injection) in the heart (0.216 %ID/g) and kidney (0.155 %ID/g); this was followed by a second peak (10–20 min after injection) in the liver (0.162 %ID/g) and the region over the stomach and spleen (0.158 %ID/g) (Fig. 3A). Thereafter, an exponential washout from the various organs over several hours was accompanied by a late peak (>15 h) in the bladder (0.135 %ID/g), indicating predominantly renal excretion of the tracer (Fig. 3B). The brain had a generally low [124I]FIAU-derived radioactivity throughout the measurement (<0.04 %ID/g in the first minutes; <0.02 %ID/g after 1 h); these values were the lowest values of all organs (Fig. 3B), indicating poor BBB penetration of [124I]FIAU.

[124I]FIAU Shows Rapid, Nonspecific Accumulation Within Recurrent Glioblastoma

To further investigate whether [124I]FIAU was taken up to significant levels within a glioblastoma, a 50-y-old patient with a recurrent glioblastoma received a bolus injection of 77.7 MBq (2.1 mCi) [124I]FIAU, and several emission scans were obtained to follow the time-dependent kinetics of tracer accumulation and washout. As depicted in Figure 4, the tumor presented as a contrast-enhancing (MRI), hypermetabolic (FDG) lesion within the left parieto-occipital lobe with increased [11C]MET uptake and gross paratumoral edema (MRI). Within the first hour after injection, [124I]FIAU was rapidly taken up within the hypermetabolic contrast-enhancing lesion and showed a wider distribution within the paratumoral edematous area at 8–24 h and a slow washout from these areas until 68 h after injection (Fig. 4). No significant [124I]FIAU uptake was found in the contralateral hemisphere.

For ROI analysis, regions were drawn on transaxial slices over the tumor, paratumoral area, gray and white matter of the contralateral hemisphere, and scalp. The kinetic analysis of [124I]FIAU revealed that maximum levels of radioactivity were reached in tumor and scalp within the first 10 min after injection (~0.001 %ID/cm³); this was followed by a continuous efflux over the 68-h study interval (Fig. 5). Tracer influx and washout from both regions followed similar kinetics. In the paratumoral edematous area, [124I]FIAU uptake was much slower than that in the tumor. In gray and white matter, [124I]FIAU uptake was also slower, and values for [124I]FIAU-derived radioactivity were always lower than the tumor values. The difference in radioactivity concentrations between tumor and normal brain tissue was larger in the beginning (factor of ~10; 0–60 min after injection) compared with that at later study times (factor of ~3; 8–68 h after injection).

A two-rate constant, one-tissue compartment model (blood and tissue) gave generally good fits to the data (Figs. 5 and 6). Fitted rate constants are given in Table 1. Among
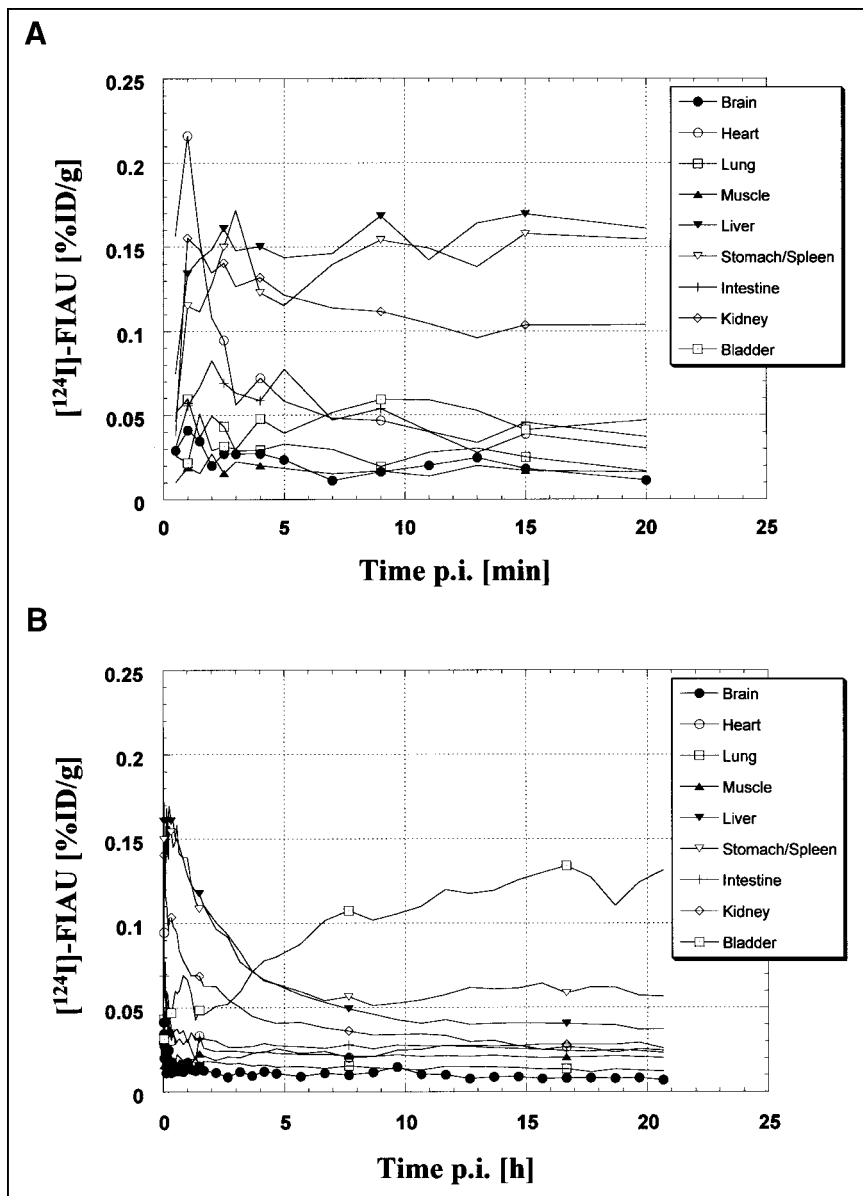
FIGURE 3. Analysis of quantitative kinetics of [^{124}I]FIAU in various organs of cats early (A) and late (B) after systemic administration of 37 MBq [^{124}I]FIAU. Values are averaged over three animals. Brain showed lowest [^{124}I]FIAU uptake of all organs throughout entire measurement. Brain symbols (●) represent PET frames acquired sequentially. For clarity in graphs, not all symbols for each frame are depicted for other organs. p.i. = after injection.

brain ROIs, K1 and k2 refer to forward and reverse transport of FIAU across the BBB. Vb is the plasma distribution volume within the tissue. The influx rate constant, K1, in these ROIs was highest for the tumor and lowest for white matter. To justify the use of a two-rate constant, one-tissue compartment model over a more complex model in this preliminary evaluation of one patient, the Akiake (AIC) and Schwartz (SC) criteria were calculated after best fits were determined for several models by minimizing a χ^2 function (*29–31*). For example, for the tumor VOI, the introduction of a k3 (0.0000294 $\pm$ 0.000018 min^{-1} in a three-rate constant, two-tissue compartment model, where k3 would refer to forward transport of FIAU into tumor cells) did not improve the respective criterion significantly (AIC$_{k1/2}$ = 12.8 vs. AIC$_{k1-k3}$ = 11.5; SC$_{k1/2}$ = 15.3 vs. SC$_{k1-k3}$ = 14.8).

Patlak analysis (Fig. 6) showed a fast initial increase in radioactivity concentration in tumor and scalp related to increased blood–tissue penetration and a slow increase in the edematous peritumoral area and normal brain tissue. After the initial influx, tissue accumulation rates reached zero for all regions, indicating the reversibility of FIAU uptake and the absence of FIAU trapping in tissue that has not been transduced by herpes viral thymidine kinase.

DISCUSSION

The main purpose of this study was to evaluate whether FIAU, the PET marker substrate of viral thymidine kinase gene expression, penetrates the BBB. Our results are limited because of the small number of subjects, but they indicate that FIAU does not penetrate the intact BBB in cat and man sufficiently, whereas significant nonspecific FIAU accumulation occurs in areas of BBB disruption accompanying a glioblastoma. In our patient, the nonspecific FIAU accumulation

MRI
(T1+Gd)

[¹¹C]-MET
[0-1.6 µCi/g]

[¹⁸F]-FDG
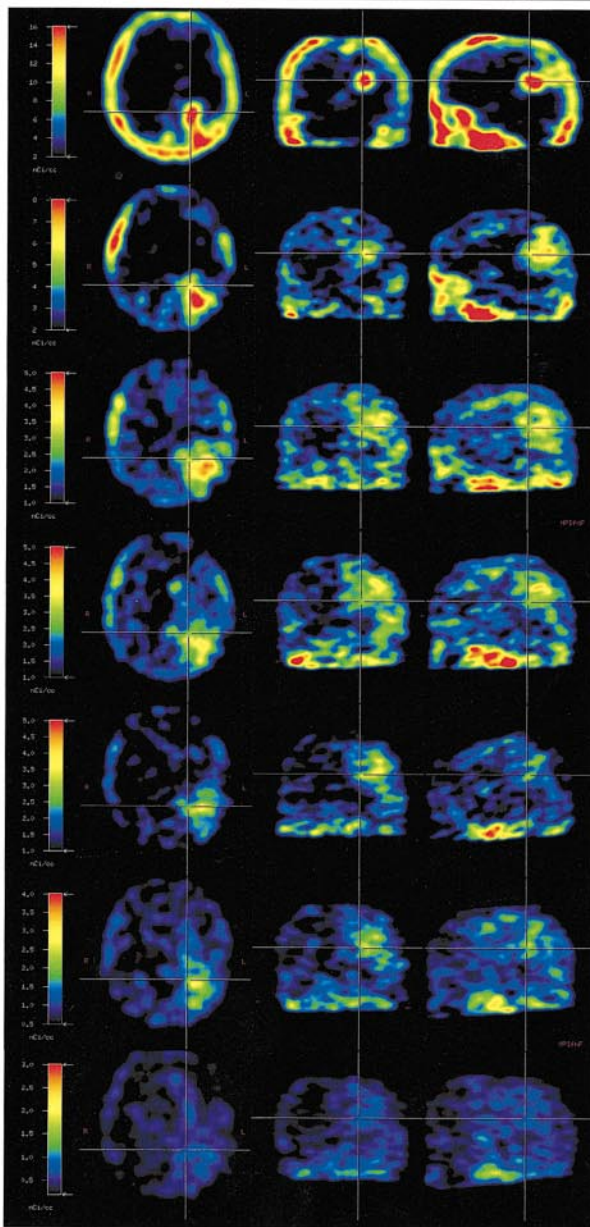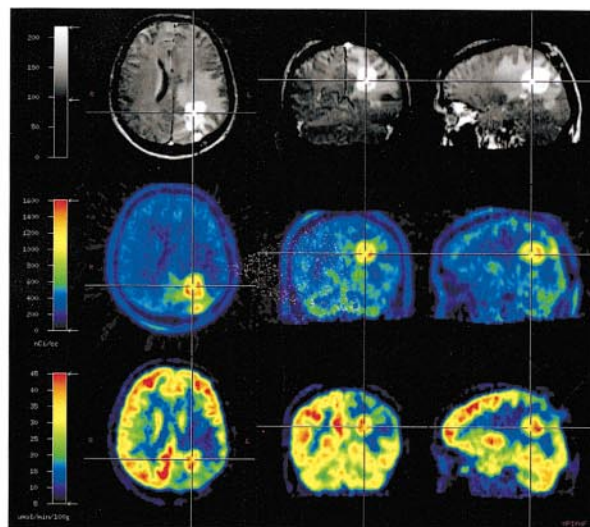[5-45 µmol/min/100g]

[¹²⁴I]-FIAU
[nCi/g]

[2-16 nCi/g] — 1 h p.i.

[2-8 nCi/g] — 8 h p.i.

[1-5 nCi/g] — 20 h p.i.

[1-5 nCi/g] — 24 h p.i.

[1-5 nCi/g] — 30 h p.i.

[0.5-4 nCi/g] — 44 h p.i.

[0.2-3 nCi/g] — 68 h p.i.

FIGURE 4. Multitracer PET and MRI of 50-y-old male patient with recurrent glioblastoma in left parieto-occipital lobe. T1-weighted MR image shows large subcortical edema within left hemisphere surrounding contrast-enhancing tumor mass. Tumor shows increased [¹¹C]MET uptake (3.1-fold higher than corresponding contralateral temporal region), high glucose consumption (37.3 µmol/100 g/min), and deactivation of surrounding cortex (62.1% of corresponding contralateral region). After systemic administration of 77 MBq [¹²⁴I]FIAU, dynamic emission sequence over 68 h shows high FIAU accumulation within tumor, scalp, and soft tissue within first hour after injection (p.i.). At later times (8–24 h after injection), substantial FIAU uptake was also observed in peritumoral edematous areas. Washout of FIAU from these regions was slow. Substantial uptake of FIAU in contralateral gray and white matter was not observed.
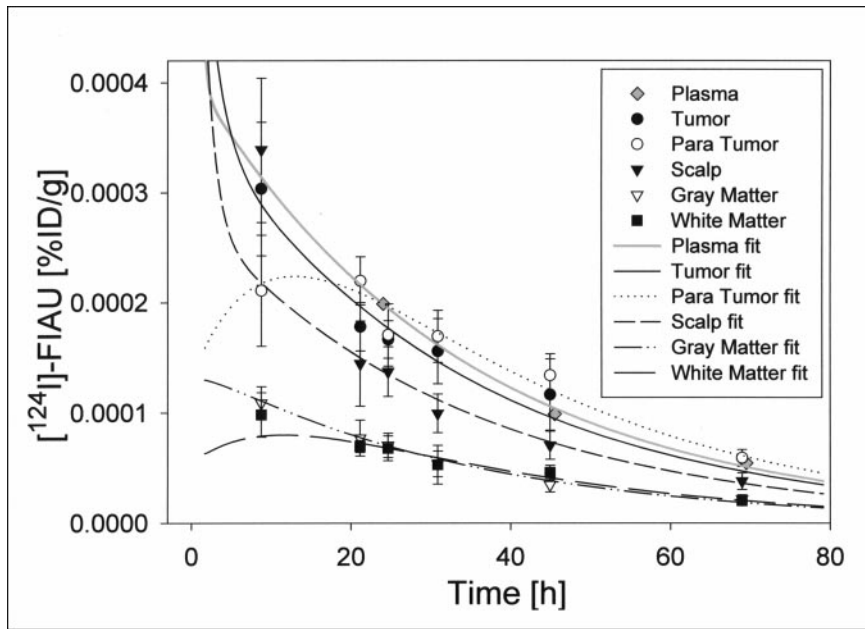
FIGURE 5. Quantitative kinetics of [124I]FIAU in plasma, scalp, tumor, paratumoral area, gray matter, and white matter of 50-y-old male patient with recurrent glioblastoma. Maximum values are reached in tumor and scalp regions within 5–10 min after injection. FIAU washout from tumor and scalp follows similar kinetics. Gray and white matter [124I]FIAU uptake values are always much lower than those in tumor. Symbols represent PET frames acquired sequentially. For clarity in graph, symbols for first 11 frames acquired during first hour after [124I]FIAU injection are omitted. Curves are model fits to data.

occurred rapidly (within 10 min after injection) in the contrast-enhancing tumor area and slower (several hours) in the area of paratumoral edema. The exponential washout of FIAU from the tumor area was slow (several days). Significant trapping of FIAU within the tumor was not observed, and no significant FIAU uptake occurred in normal brain tissue.

Our data are consistent with dosimetry estimates obtained from the distribution of [124I]FIAU-derived radioactivity in
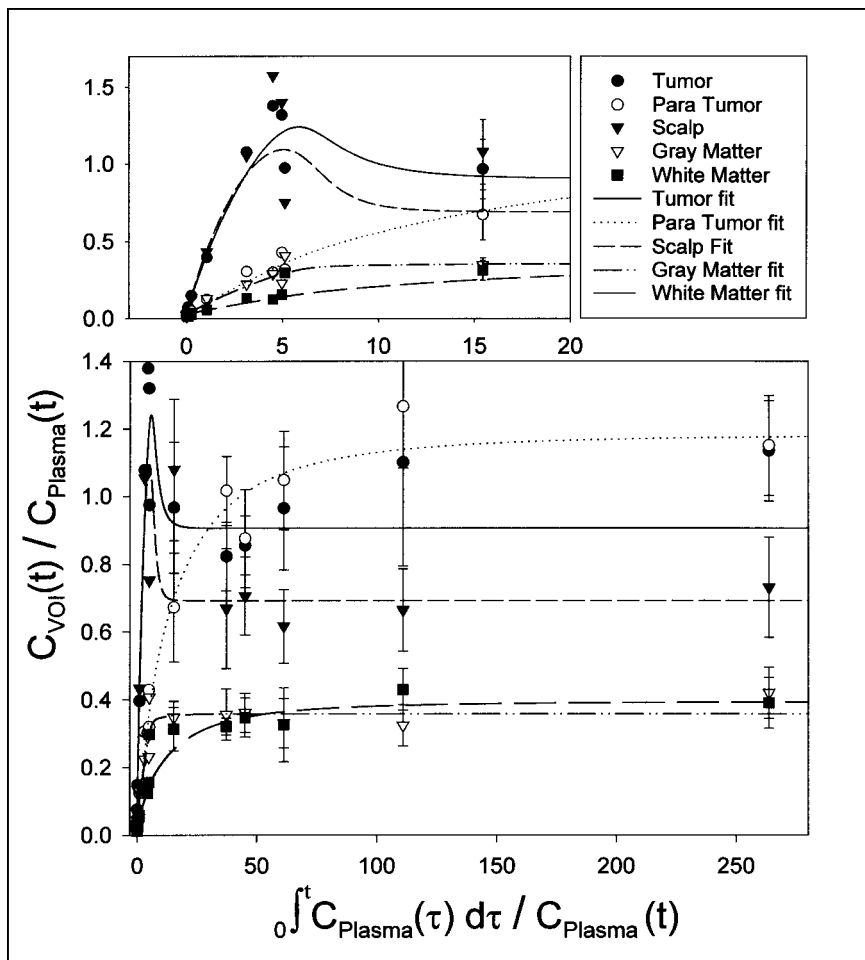

FIGURE 6. Patlak plots of FIAU uptake in various tissues of 50-y-old male patient with recurrent glioblastoma show fast initial uptake of FIAU in tumor and scalp but no FIAU accumulation or trapping in any tissue. Curves are model fits to data.

TABLE 1
Fitted FIAU Rate Constants Generated from Tissue Time–Activity Curves in Various Tissue Regions of Patient with Recurrent Glioblastoma

Region	K1* (mL/min/g)	k2* (min^{-1})	Vb† (%)
Tumor	0.0071 ± 0.0018	0.009 ± 0.002	4.2 ± 1.4
Paratumor	0.00124 ± 0.00001	0.00157 ± 0.00001	2.75 ± 0.03
Scalp	0.009 ± 0.002	0.014 ± 0.003	1.8 ± 1.0
Gray matter	0.0012 ± 0.0005	0.0041 ± 0.0016	2.9 ± 0.9
White matter	0.00042 ± 0.00012	0.0017 ± 0.0005	3.0 ± 0.8

*K1 and k2 refer to forward and reverse transport of FIAU across BBB.
†Vb is plasma distribution volume within tissue.
Data are presented as mean ± SD from nonlinear least-squares fit.

various organs and tissues from rats injected with diagnostic doses of [124I]FIAU (12). Thirty-six hours after intravenous administration of 50 μCi [124I]FIAU, the authors found the lowest retained radioactivity values within the brain (0.0004 %ID/g) and muscle (0.0019 %ID/g), followed by the gonads (0.0023 %ID/g), heart (0.0035 %ID/g), and the stomach, bladder, liver, kidney, large intestine, spleen, and small intestine (0.0111–0.0192 %ID/g) in ascending order. Bone marrow and thyroid revealed the highest levels of retained radioactivity (0.0211 and 1.1133 %ID/g, respectively). Twenty-two hours after intravenous administration of 37MBq [124I]FIAU in cats, we found the lowest values in the brain (0.0069 %ID/g), lung (0.0123 %ID/g), and muscle (0.0201 %ID/g), followed by the intestine, heart and kidney (0.0231–0.0257 %ID/g), liver (0.037 %ID/g), stomach and spleen (0.057 %ID/g) and the highest values in the bladder (0.131 %ID/g). Because of limited spatial resolution, small organs or tissues, such as bone marrow and thyroid, could not be assessed. In contrast with tissue sampling, this in vivo study facilitated the assessment of the kinetics of [124I]FIAU distribution within organs over time. Organs with fast (heart, kidney), intermediate (liver, stomach and spleen), slow (bladder), and nearly no (brain, muscle) [124I]FIAU uptake could be easily identified. Whole-body PET scanning thus enables a detailed analysis of time course variations of tracer distribution within different organs. In this respect, PET in cats using a clinical scanner seems well suited for the study of tracer kinetics in general because whole-body scans can be obtained in a species just large enough to allow easy demarcation and analysis of the most relevant organs.

Both the cited studies and our study suggest that [124I]FIAU uptake in the healthy brain with an intact BBB is very low. Therefore, [124I]FIAU does not meet one essential criterion for an ideal marker substrate for noninvasive imaging of gene expression using a radiotracer assay, which is free penetration of the BBB and cell membranes (6). The limited BBB permeability of [124I]FIAU is in contrast with previous suggestions that the lipophilic properties of fluorinated pyrimidines such as FIAU predict good BBB penetration (20,21).

Our preliminary pharmacokinetic model (one patient) for FIAU and the Patlak analysis reveal a fast and relatively high but nonspecific FIAU accumulation in the area of a glioblastoma. Together with the high metabolic stability of FIAU, this suggests that FIAU may still be of value as a PET marker substrate in gene therapy for brain tumors provided the BBB is disrupted. The plasma half-life of therapeutic doses of FIAU is ~3.9 h after systemic administration of the related pyrimidine 2-fluoro-2-deoxy-β-D-arabinofuranosyl-5-iodocytosine, which functions as a prodrug for FIAU (20,32), and 29.3 h after oral administration of a single 5-mg dose of FIAU (33). FIAU is cleared from plasma mainly by renal elimination. Further biotransformation is limited because of the high chemical and metabolic stability of the N-glycosyl linkage in pyrimidine nucleosides that contain the 2′-fluoro substituent in the arabinosyl ("up") configuration (21,34,35). Only minor metabolism has been reported to occur as deiodination to FAU with subsequent methylation to 2-fluoro-2-deoxy-β-D-arabino-furanosylthymine by thymidylate synthase (36,37) or to an unknown glucuronide, most likely at the 5′ position (32). The in vitro and in vivo stability of [131I]FIAU was investigated in serum and whole blood (38). Over a 24-h period, 97.8% ± 0.1% of labeled compound remained unchanged, indicating excellent stability and low susceptibility to deiodination (38). As a result of its stability, nondegraded radiolabeled FIAU may serve as a potential PET marker substrate in target tissue that has been transduced by gene therapy. Confounding problems associated with imaging radiolabeled metabolites in both target and surrounding tissues are avoided, which has led to the investigation of FIAU for imaging herpes encephalitis (39,40) and HSV-1-*tk* gene expression in vivo (8,9,11,12,16).

CONCLUSION

[124I-]FIAU is a promising 124I-labeled nucleoside analog for imaging herpes viral thymidine kinase gene expression. Whereas clinically relevant levels of HSV-1-*tk* gene expression within brain tumors with BBB disruption or in organs outside the CNS might be imaged by FIAU PET, [124I]FIAU may not be the marker substrate of choice for the noninvasive localization of HSV-1-*tk* gene expression in the CNS

under conditions in which the BBB is most likely to be intact.

ACKNOWLEDGMENTS

REFERENCES

1. Young AB. Neurological disorders: an overview. In: Chiocca EA, Breakefield XO, eds. *Gene Therapy for Neurological Disorders and Brain Tumors*. Totowa, NJ: Humana Press; 1998:341–343.

2. Ram Z, Culver KW, Oshiro EM, et al. Therapy of malignant brain tumors by intratumoral implantation of retroviral vector-producing cells. *Nat Med*. 1997;3:1354–1361.

3. Shand N, Weber F, Mariani L, et al. A phase 1–2 clinical trial of gene therapy for recurrent glioblastoma multiforme by tumor transduction with the herpes simplex thymidine kinase gene followed by ganciclovir: GLI328 European-Canadian Study Group. *Hum Gene Ther*. 1999;10:2325–2335.

4. Gambhir SS, Barrio JR, Wu L, et al. Imaging of adenoviral-directed herpes simplex virus type 1 thymidine kinase reporter gene expression in mice with radiolabeled ganciclovir. *J Nucl Med*. 1998;39:2003–2011.

5. Jacobs A, Dubrovin M, Hewett J, et al. Functional co-expression of HSV-1 thymidine kinase and green fluorescent protein: implications for non-invasive imaging of transgene expression. *Neoplasia*. 1999;1:154–161.

6. Tjuvajev JG, Stockhammer G, Desai R, et al. Imaging the expression of transfected genes in vivo. *Cancer Res*. 1995;55:6126–6132.

7. Hollen T. Researchers and regulators reflect on first gene therapy death. *Nat Med*. 2000;6:6.

8. Gambhir SS, Barrio JR, Phelps ME, et al. Imaging adenoviral-directed reporter gene expression in living animals with positron emission tomography. *Proc Natl Acad Sci USA*. 1999;96:2333–2338.

9. Gambhir SS, Bauer E, Black ME, et al. A mutant herpes simplex virus type 1 thymidine kinase reporter gene shows improved sensitivity for imaging reporter gene expression with positron emission tomography. *Proc Natl Acad Sci USA*. 2000;97:2785–2790.

10. Gambhir SS, Herschman HR, Cherry SR, et al. Imaging transgene expression with radionuclide technologies. *Neoplasia*. 2000;2:118–138.

11. Tjuvajev JG, Finn R, Watanabe K, et al. Noninvasive imaging of herpes virus thymidine kinase gene transfer and expression: a potential method for monitoring clinical gene therapy. *Cancer Res*. 1996;56:4087–4095.

12. Tjuvajev JG, Avril N, Oku T, et al. Imaging herpes virus thymidine kinase gene transfer and expression by positron emission tomography. *Cancer Res*. 1998;58:4333–4341.

13. Tjuvajev JG, Chen SH, Joshi A, et al. Imaging adenoviral-mediated herpes virus thymidine kinase gene transfer and expression in vivo. *Cancer Res*. 1999;59:5186–5193.

14. Bogdanov AJ, Weissleder R. The development of in vivo imaging systems to study gene expression. *Trends Biotechnol*. 1998;16:5–10.

15. Weissleder R, Moore A, Mahmood U, et al. In vivo magnetic resonance imaging of transgene expression. *Nat Med*. 2000;6:351–355.

16. Jacobs A, Tjuvajev JG, Balatoni J, et al. Imaging HSV-1 vector mediated gene expression in vivo [abstract]. *J Cereb Blood Flow Metab*. 1999;19(suppl):S294.

17. Colacino JM. Mechanisms for the anti-hepatitis B virus activity and mitochondrial toxicity of fialuridine (FIAU). *Antiviral Res*. 1996;29:125–139.

18. Lewis W, Dalakas MC. Mitochondrial toxicity of antiviral drugs. *Nat Med*. 1995;1:417–422.

19. McKenzie R, Fried MW, Sallie R, et al. Hepatic failure and lactic acidosis due to fialuridine (FIAU), an investigational nucleoside analogue for chronic hepatitis B. *N Engl J Med*. 1995;333:1099–1105.

20. King DH. Fluorinated pyrimidines: a new chance for old drugs. *Transplant Proc*. 1991;23(suppl 3):168–170.

21. Philips FS, Feinberg A, Chou TC, et al. Distribution, metabolism, and excretion of 1-(2-fluoro-2-deoxy-beta-D-arabinofuranosyl)thymine and 1-(2-fluoro-2-deoxy-beta-D-arabinofuranosyl)-5-iodocytosine. *Cancer Res*. 1983;43:3619–3627.

22. Tovell DR, Samuel J, Mercer JR, et al. The in vitro evaluation of nucleoside analogues as probes for use in the noninvasive diagnosis of herpes simplex encephalitis. *Drug Des Deliv*. 1988;3:213–221.

23. Weinreich R, Knust EJ. Quality assurance of iodine-124 produced via the nuclear reaction [124]Te(d,2n)[124]I. *J Radioanal Nucl Chem Lett*. 1996;213:253–261.

24. Pietrzyk U, Herholz K, Fink G, et al. An interactive technique for three-dimensional image registration: validation for PET, SPECT, MRI and CT brain studies. *J Nucl Med*. 1994;35:2011–2018.

25. Heiss WD, Graf R, Wienhard K, et al. Dynamic penumbra demonstrated by sequential multitracer PET after middle cerebral artery occlusion in cats. *J Cereb Blood Flow Metab*. 1994;14:892–902.

26. Herholz K, Holzer T, Bauer B, et al. ^{11}C-methionine PET for differential diagnosis of low-grade gliomas. *Neurology*. 1998;50:1316–1322.

27. Wurker M, Herholz K, Voges J, et al. Glucose consumption and methionine uptake in low-grade gliomas after iodine-125 brachytherapy. *Eur J Nucl Med*. 1996;23:583–586.

28. Wienhard K, Dahlbom M, Eriksson L, et al. The ECAT EXACT HR: performance of a new high resolution positron scanner. *J Comput Assist Tomogr*. 1994;18:110–118.

29. Wienhard K, Herholz K, Coenen HH, et al. Increased amino acid transport into brain tumors measured by PET of L-(2-^{18}F)fluorotyrosine. *J Nucl Med*. 1991;32:1338–1346.

30. Marquardt M. An algorithm for least-squares estimation of nonlinear parameters. *J Soc Ind Appl Math*. 1963;11:431–441.

31. Patlak CS, Blasberg RG, Fenstermacher JD. Graphical evaluation of blood-to-brain transfer constants from multiple-time uptake data. *J Cereb Blood Flow Metab*. 1983;3:1–7.

32. Feinberg A, Leyland-Jones B, Fanucchi MP, et al. Biotransformation and elimination of [2-^{14}C]-1-(2-deoxy-2′-fluoro-beta-D-arabinofuranosyl)-5-iodocytosine in immunosuppressed patients with herpesvirus infections. *Antimicrob Agents Chemother*. 1985;27:733–738.

33. Bowsher RR, Compton JA, Kirkwood JA, et al. Sensitive and specific radioimmunoassay for fialuridine: initial assessment of pharmacokinetics after single oral doses to healthy volunteers. *Antimicrob Agents Chemother*. 1994;38:2134–2142.

34. Chou TC, Feinberg A, Grant AJ, et al. Pharmacological disposition and metabolic fate of 2′-fluoro-5-iodo-1-beta-D-arabinofuranosylcytosine in mice and rats. *Cancer Res*. 1981;41:3336–3342.

35. Watanabe KA, Reichman U, Hirota K, Lopez C, Fox JJ. Nucleosides: 110—Synthesis and antiherpes virus activity of some 2′-fluoro-2′-deoxyarabinofuranosylpyrimidine nucleosides. *J Med Chem*. 1979;22:21–24.

36. Cui L, Yoon S, Schinazi RF, Sommadossi JP. Cellular and molecular events leading to mitochondrial toxicity of 1-(2-deoxy-2-fluoro-1-beta-D-arabinofuranosyl)-5-iodouracil in human liver cells. *J Clin Invest*. 1995;95:555–563.

37. Klecker RW, Katki AG, Collins JM. Toxicity, metabolism, DNA incorporation with lack of repair, and lactate production for 1-(2′-fluoro-2′-deoxy-beta-D-arabinofuranosyl)-5-iodouracil in U-937 and MOLT-4 cells. *Mol Pharmacol*. 1994;46:1204–1209.

38. Vaidyanathan G, Zalutsky MR. Preparation of 5-[^{131}I]iodo- and 5-[[211]At]astato-1-(2-deoxy-2-fluoro-beta-D-arabinofuranosyl)uracil by a halodestannylation reaction. *Nucl Med Biol*. 1998;25:487–496.

39. Iwashina T, Tovell DR, Xu L, Tyrrell DL, Knaus EE, Wiebe LI. Synthesis and antiviral activity of IVFRU, a potential probe for the non-invasive diagnosis of herpes simplex encephalitis. *Drug Des Deliv*. 1988;3:309–321.

40. Saito Y, Price RW, Rottenberg DA, et al. Quantitative autoradiographic mapping of herpes simplex virus encephalitis with a radiolabeled antiviral drug. *Science*. 1982;217:1151–1153.